Dynamics of a rigid body in a Stokes fluid

O. Gonzalez*, A.B.A. Graf and J.H. Maddocks†

July 11, 2003

Abstract

We demonstrate that the dynamics of a rigid body falling in an infinite, viscous fluid can, in the Stokes limit, be reduced to the study of a three-dimensional system of ordinary differential equations $\dot{\eta} = \eta \times M_2 \eta$ where $M_2 \in \mathbb{R}^{3\times 3}$ is a generally non-symmetric matrix containing certain hydrodynamic mobility coefficients. We further show that all steady states and their stability properties can be classified in terms of the Schur form of M_2. Steady states correspond to screw motions (or limits thereof) in which the center of mass traces a helical path, while the body spins uniformly about the vertical. All rigid bodies have at least one such stable, screw motion. Bodies for which M_2 has exactly one real eigenvalue have a unique, globally attracting, asymptotically stable screw motion, while other bodies can have multiple, stable and unstable steady motions. One application of our theory is to the case of rigid filaments, which in turn is a first step in modeling the sedimentation rate of flexible polymers such as DNA. For rigid filaments the matrix M_2 can be approximated using the Rotne-Prager theory, and we present various examples corresponding to certain *ideal* shapes of knots which illustrate the various possible multiplicities of steady states. Our simulations of rigid ideal knots in a Stokes fluid predict an approximate linear relation between sedimentation speed and average crossing number, as has been observed experimentally for the much more complicated system of real DNA knots in gel electrophoresis.

1 Introduction

In this article we study the sedimentation dynamics of a rigid body in a viscous fluid (of infinite extent and at rest at infinity) under the effects of a uniform, external body force such as gravity. According to the classic Stokes approximation for low Reynolds number flow, the drag force and torque exerted by a viscous fluid on a slowly moving, immersed rigid body can be determined from its linear and angular velocities via linear relations whose coefficients depend only upon the shape of the body [4, 10, 2]. In particular, the non-local effects

*Department of Mathematics, University of Texas, Austin, TX 78712, og@math.utexas.edu

†Institut Mathématiques Bernoulli, École Polytechnique Fédérale de Lausanne, CH-1015 Lausanne, Switzerland, arnulf.graf@tuebingen.mpg.de, john.maddocks@epfl.ch

of the fluid upon the body are described by a symmetric, sign-definite hydrodynamic resistance matrix. This fact allows the equations of motion for the body and fluid to be decoupled, and the motion of the body may be studied without explicit consideration of the fluid.

Assuming the body force is small compared to the fluid viscosity, we use singular perturbation techniques to develop a description of the leading-order body dynamics. We show that leading-order motions are completely characterized by a generalized Euler equation of the form

$$\dot{\eta} = \eta \times M_2 \eta, \tag{1}$$

where $\eta \in \mathbb{R}^3$ are the components of the body force in the body frame and $M_2 \in \mathbb{R}^{3\times 3}$ is a matrix containing certain hydrodynamic mobility coefficients that will be defined later. The study of equation (1) in the case that the matrix M_2 is symmetric (and with entirely different interpretations of the variables) is a classic problem of mechanics, see for example [11]. However in our context the matrix M_2 is generally non-symmetric, and the corresponding solution set is quite different from the classic case. Dependent upon the properties of M_2, equation (1) shows that a rigid body may admit a range of different unsteady motions, together with a number of different steady states. In particular, each real eigenvector of M_2 defines a hydrodynamic axis in the body and gives rise to a pair of steady states. The two states in a pair correspond to screw motions in which the hydrodynamic axis remains parallel to the external force field with either the same or opposite orientation, while the center of mass traces out a helical path about an axis that is also parallel to the external force field. Furthermore, the screw motions are necessarily one of four possible types: a general helical spin or one of the three degenerate limits of a vertical spin, a vertical translation or a non-vertical translation.

We give a complete classification of all steady states and their stability properties for bodies that are generic in an appropriate sense. Our analysis shows that every generic body has either two or six distinct steady states depending on whether M_2 has either one or three real eigenvalues. In the first case we find that one state is stable and the other is unstable. The stable state has the property that it is the limit of all motions except for the unstable state, and for this reason we refer to it as being globally asymptotically stable. In the second case we find that two steady motions are stable and four are unstable. In this case both of the stable states are locally asymptotically stable. Moreover, we present numerical examples of bodies, actually rigid filaments with mobility coefficients computed in the Rotne-Prager approximation [13], with exactly two and with exactly six steady states.

We further exploit our perturbation results to characterize the sedimentation speed of an arbitrary rigid body in any motion, steady or not. We demonstrate that the speed of the body mass center in a direction parallel to the external force field is, after a short interval of time, described by a quadratic form defined by a certain constant symmetric matrix $M_1 \in \mathbb{R}^{3\times 3}$. As a consequence, the sedimentation speed of a body is bounded above and below, respectively, by the maximum and minimum eigenvalues of M_1. Thus, while sedimentation speed in general depends upon the initial conditions of the motion and may vary with time, it must do so between constant bounds determined by intrinsic properties of the body and the strength of the external force field. For a given body it is desirable to introduce a characteristic value of the sedimentation speed that is independent of initial conditions. Our result shows that different characteristic values may be defined in terms of the matrix M_1.

Many aspects of the dynamics of a rigid body in a Stokes fluid have been studied before [4, 18, 2]. Happel and Brenner [4] studied spin-free translational steady states for arbitrary bodies and characterized their static stability in the sense of buoyancy theory. Weinberger [18] proved that bodies whose center of mass and center of volume are sufficiently separated possess a steady state that is globally asymptotically stable, and further showed that the corresponding sedimentation speed for this steady state may be bounded by means of several variational principles. More recently, Galdi [2] has studied the steady states of homogeneous bodies of revolution with fore-and-aft symmetry for both Stokes and Navier-Stokes fluid models.

In this article we characterize all possible steady states for an arbitrary rigid body in a Stokes fluid. For bodies that are generic in an appropriate sense, we determine the precise numbers of steady states they possess, and characterize the (non-linear) stability properties of the steady motions using Lyapunov function techniques. Furthermore, we find bounds on the sedimentation speed for an arbitrary body in any motion for which the fluid may be modeled using the steady Stokes equations. All our results are first developed for bodies under the assumption that their center of mass and center of volume are coincident, as is the case for bodies with uniform mass density. We then show how these results extend in a straightforward way to the general case when their center of mass and center of volume are distinct, which is typical for bodies with non-uniform mass density.

As an application of our theory we consider the case when the rigid body is a closed loop formed from a tube of small radius, and numerically compute the associated hydrodynamic resistance matrix using the methods outlined in [3]. In particular, the continuous tube is replaced by a collection of beads or spheres along the tube centerline and their hydrodynamic interaction is determined using the Rotne-Prager approximation [13]. We use resistance matrices approximated in this way to simulate numerically the sedimentation dynamics of rigid, knotted filaments. We present various examples corresponding to certain *ideal* shapes of knots [7, 8] which illustrate the various possible multiplicities of steady states and their stability. Moreover, our simulations of ideal knots in a Stokes fluid predict that there is an approximate linear relation between sedimentation speed and average crossing number, as has been observed experimentally for real DNA knots in gel electrophoresis [16, 17]. In particular, rigid filaments of the same length, radius and mass exhibit different characteristic sedimentation speeds depending on their knot type.

The presentation is structured as follows. In Section 2 we outline the equations governing the dynamics of a rigid body in low Reynolds number flow when the centers of mass and volume are coincident. In Section 3 we non-dimensionalize these equations and show that they are singularly perturbed when the body force is small compared to the fluid viscosity in an appropriate sense. We perform a singular perturbation analysis and establish various properties of the leading-order dynamics. In Section 4 we characterize all possible steady states of the leading-order system and derive criteria that characterize their stability. In Section 5 we use our leading-order solution to develop bounds on the sedimentation speed of a body in any motion. In Section 6 we apply our theory to the case of rigid filaments and present various numerical examples involving knotted filaments in their ideal geometrical forms. Finally, in Section 7 we drop the assumption that the centers of mass and volume are coincident, and show that all our results carry over to the general case in which they are distinct.

2 Rigid body kinematics and balance laws

We consider a general rigid body whose configuration is defined by a vector $\boldsymbol{r}$ and an orthonormal frame $\{\boldsymbol{d}_i\}$ $(i = 1, 2, 3)$. The vector $\boldsymbol{r}$ describes the position of the body mass center, while the frame $\{\boldsymbol{d}_i\}$ is fixed in the body and describes its orientation relative to a frame $\{\boldsymbol{e}_i\}$ fixed in space. The kinematics of the body are encapsulated in the vector relations

$$\dot{\boldsymbol{r}} = \boldsymbol{v}, \qquad \dot{\boldsymbol{d}}_i = \boldsymbol{\omega} \times \boldsymbol{d}_i \quad (i = 1, 2, 3), \tag{2}$$

where $\boldsymbol{v}$ is the linear velocity of the mass center and $\boldsymbol{\omega}$ is the angular velocity of the body frame.

The linear momentum $\boldsymbol{p}$ and angular momentum $\boldsymbol{\pi}$ of the body about its mass center are given by the vector relations

$$\boldsymbol{p} = m\boldsymbol{v}, \qquad \boldsymbol{\pi} = \boldsymbol{C}\boldsymbol{\omega}, \tag{3}$$

where m is the total mass, and $\boldsymbol{C}$ is the (symmetric, positive-definite) rotational inertia tensor with respect to the mass center. When the body is acted upon by a system of loads with resultant force $\boldsymbol{f}$ and resultant moment $\boldsymbol{\tau}$ about the mass center, the balance laws for linear and angular momentum take the form

$$\dot{\boldsymbol{p}} = \boldsymbol{f}, \qquad \dot{\boldsymbol{\pi}} = \boldsymbol{\tau}. \tag{4}$$

We suppose that the body is immersed in an unbounded, uniform, viscous fluid and is moving under the action of a uniform gravitational field. For simplicity we initially assume that the center of mass of the body coincides with its center of volume, as is the case when the mass density of the body is also uniform. Then the net effects of gravitational and hydrostatic (or buoyancy) forces acting on the body are given by the resultants

$$\boldsymbol{f}^{(s)} = \boldsymbol{\eta}, \qquad \boldsymbol{\tau}^{(s)} = \boldsymbol{0}, \tag{5}$$

where $\boldsymbol{\eta} = \alpha \boldsymbol{e}_3$ is a prescribed vector, independent of the body position and orientation, that is parallel to the unit vertical $\boldsymbol{e}_3$, and with given norm $|\alpha| > 0$.

We further assume that the resultant force and moment about the mass center of all hydrodynamic, velocity-dependent drag forces on the body surface are linearly related to the velocities:

$$\boldsymbol{f}^{(d)} = -\boldsymbol{L}_1 \boldsymbol{v} - \boldsymbol{L}_3 \boldsymbol{\omega}, \qquad \boldsymbol{\tau}^{(d)} = -\boldsymbol{L}_2 \boldsymbol{v} - \boldsymbol{L}_4 \boldsymbol{\omega}, \tag{6}$$

where $\boldsymbol{L}_a$ $(a = 1, \dots, 4)$ are given hydrodynamic resistance tensors. These linear relations are consistent with the assumption that the viscous fluid surrounding the body may be described by the standard (steady) Stokes flow equations [4, 10, 2], where the fluid velocity field is assumed to vanish at infinity.

The balance equations then take the form

$$\begin{array}{rcl} \dot{\boldsymbol{\eta}} & = & \boldsymbol{0}, \\ \dot{\boldsymbol{p}} & = & -\boldsymbol{L}_1 \boldsymbol{v} - \boldsymbol{L}_3 \boldsymbol{\omega} + \boldsymbol{\eta}, \\ \dot{\boldsymbol{\pi}} & = & -\boldsymbol{L}_2 \boldsymbol{v} - \boldsymbol{L}_4 \boldsymbol{\omega}, \end{array} \tag{7}$$

where $(7)_1$ expresses constancy of the vector $\boldsymbol{\eta}$, while $(7)_{2,3}$ are obtained by substitution of (6) and (5) into (4). When expressed in terms of components with respect to the body frame $\{\boldsymbol{d}_i\}$, i.e., $L_1^{ij} = \boldsymbol{d}_i \cdot \boldsymbol{L}_1 \boldsymbol{d}_j$, $\eta_i = \boldsymbol{\eta} \cdot \boldsymbol{d}_i$ and so on, we find that the equations in (7) become

$$\begin{array}{rcl} \dot{\eta} + \omega \times \eta & = & 0, \\ \dot{p} + \omega \times p & = & -L_1 v - L_3 \omega + \eta, \\ \dot{\pi} + \omega \times \pi & = & -L_2 v - L_4 \omega, \end{array} \tag{8}$$

where $v = m^{-1} p$ and $\omega = C^{-1} \pi$. Here we use the notation $\eta = (\eta_i) \in \mathbb{R}^3$ and $C = (C_{ij}) \in \mathbb{R}^{3\times 3}$ for component vectors and matrices.

The hydrodynamic resistance matrices L_a depend on the shape of the rigid body and are proportional to the (absolute) viscosity μ of the fluid. The reason for considering the balance laws (7) in the body frame is that when expressed in that basis the component matrices $L_a = (L_a^{ij}) \in \mathbb{R}^{3\times 3}$ are constants. General considerations show that the overall resistance matrix $L \in \mathbb{R}^{6\times 6}$ defined by

$$L = \begin{pmatrix} L_1 & L_3 \\ L_2 & L_4 \end{pmatrix} \tag{9}$$

is symmetric [4, 10, 2]. Furthermore, strict dissipation of the total rigid body energy requires that L be positive-definite. Explicit expressions for this matrix are known in only a few special circumstances, for example when the body is a sphere. However, approximations for L may be constructed by various modeling techniques [4, 10, 3], or by exploiting fundamental (singular) solutions of the Stokes equations as done in slender-body theory [1, 9].

Throughout our developments we denote the inverse of L by M so that

$$M = \begin{pmatrix} M_1 & M_3 \\ M_2 & M_4 \end{pmatrix} = \begin{pmatrix} L_1 & L_3 \\ L_2 & L_4 \end{pmatrix}^{-1}. \tag{10}$$

The block entries $M_a \in \mathbb{R}^{3\times 3}$ are typically called the hydrodynamic mobility matrices and are related to the resistance matrices $L_a \in \mathbb{R}^{3\times 3}$ through the expressions

$$\begin{aligned} M_1 &= \quad L_1^{-1} + L_1^{-1}L_3S^{-1}L_2L_1^{-1}, & M_3 &= -L_1^{-1}L_3S^{-1}, \\ M_2 &= -S^{-1}L_2L_1^{-1}, & M_4 &= \quad S^{-1}, \end{aligned} \tag{11}$$

where $S = L_4 - L_2L_1^{-1}L_3$ is the Schur complement of L_1 in L. Since L is symmetric, positive-definite, we find that M is also symmetric, positive-definite. In particular, the block entries L_1, L_4, M_1 and M_4 are all symmetric, positive-definite.

3 Singular perturbation analysis

Here we perform a singular perturbation analysis of the equations of motion (8). We first non-dimensionalize the equations and show that they are singularly perturbed when the fluid viscosity μ is large compared to the external load parameter $|\alpha|$ and body mass m in the sense that $\varepsilon = m|\alpha|/\mu^2 l^3 \ll 1$ where l is a characteristic length scale for the body. We then apply the method of matched asymptotic expansions to construct a complete description of the leading-order dynamics.

3.1 Physical parameters and time scales

Physical parameters that are relevant to (8) are the body mass $m > 0$, a body characteristic length $l > 0$, the fluid (absolute) viscosity $\mu > 0$ and the external load magnitude $|\alpha| > 0$. A dimensional analysis of these parameters leads to various characteristic time scales (only two of which are independent):

$$t_a = \sqrt{\frac{ml}{|\alpha|}}, \qquad t_b = \frac{m}{l\mu}, \qquad t_c = \frac{l^2\mu}{|\alpha|}. \tag{12}$$

The time scale t_c will be used in our analysis of (8) since it is related to settling phenomena. In particular, under the Stokes approximation the terminal settling velocity of a rigid sphere of radius l in a fluid of viscosity μ subject to a driving force of magnitude $|\alpha|$ would be proportional to l/t_c.

3.2 Non-dimensionalization

Let t_c be defined as in (12) and consider the non-dimensional time $\bar{t} = t/t_c$, the non-dimensional variables

$$\bar{\omega} = t_c\omega, \quad \bar{v} = (t_c/l)v, \quad \bar{p} = (t_c/lm)p, \quad \bar{\pi} = (t_c/l^2m)\pi, \quad \bar{\eta} = (t_c/l^2\mu)\eta,$$

the non-dimensional inertia parameters $\bar{m} = 1$, $\bar{C} = (1/l^2m)C$, and the non-dimensional resistance matrices

$$\bar{L}_1 = (1/l\mu)L_1, \quad \bar{L}_2 = (1/l^2\mu)L_2, \quad \bar{L}_3 = (1/l^2\mu)L_3, \quad \bar{L}_4 = (1/l^3\mu)L_4.$$

Substitution of the above quantities into (8) yields

$$
\begin{array}{rcl}
\dot{\bar{\eta}} + \bar{\omega} \times \bar{\eta} & = & 0, \\
\varepsilon[\dot{\bar{p}} + \bar{\omega} \times \bar{p}] & = & -\bar{L}_1 \bar{v} - \bar{L}_3 \bar{\omega} + \bar{\eta}, \\
\varepsilon[\dot{\bar{\pi}} + \bar{\omega} \times \bar{\pi}] & = & -\bar{L}_2 \bar{v} - \bar{L}_4 \bar{\omega},
\end{array}
\tag{13}
$$

where superposed dots now denote derivatives with respect to the independent variable $\bar{t}$. Here $\bar{v} = \bar{m}^{-1}\bar{p}$, $\bar{\omega} = \bar{C}^{-1}\bar{\pi}$ and $\varepsilon = m|\alpha|/\mu^2 l^3$ is a non-dimensional parameter. Notice that (13) is a singularly perturbed system of ordinary differential equations in the limit of large viscosity when $0 < \varepsilon \ll 1$.

3.3 Leading-order solution

Omitting the overbars in (13) for clarity of notation, we consider an initial value problem for $\eta(t)$, $p(t)$, $\pi(t) \in \mathbb{R}^3$ of the form

$$
\begin{array}{rcl}
\dot{\eta} + \omega \times \eta & = & 0, \\
\varepsilon[\dot{p} + \omega \times p] & = & -L_1 v - L_3 \omega + \eta, \\
\varepsilon[\dot{\pi} + \omega \times \pi] & = & -L_2 v - L_4 \omega, \\
\multicolumn{3}{c}{\eta(0) = \eta_0, \quad p(0) = p_0, \quad \pi(0) = \pi_0,}
\end{array}
\tag{14}
$$

where η_0, p_0 and π_0 are specified initial conditions. Using standard singular perturbation techniques [5], we find that a uniform leading-order solution for (14) is given by

$$
\left\{ \begin{array}{c} p(t) \\ \pi(t) \end{array} \right\} = \exp(-At/\varepsilon) \left\{ \begin{array}{c} p_0 - mM_1\eta_0 \\ \pi_0 - CM_2\eta_0 \end{array} \right\} + \left\{ \begin{array}{c} mM_1\eta(t) \\ CM_2\eta(t) \end{array} \right\}, \tag{15}
$$

where $\eta(t)$ satisfies the initial value problem

$$
\begin{array}{rcl}
\dot{\eta} & = & \eta \times M_2 \eta, \\
\eta(0) & = & \eta_0.
\end{array}
\tag{16}
$$

Here $A \in \mathbb{R}^{6\times 6}$ is defined by

$$
A = \begin{pmatrix} L_1 & L_3 \\ L_2 & L_4 \end{pmatrix} \begin{pmatrix} m^{-1}I & O \\ O & C^{-1} \end{pmatrix}. \tag{17}
$$

Notice that A has positive, real eigenvalues since it is the product of two symmetric, positive-definite matrices and that

$$
A^{-1} = \begin{pmatrix} mI & O \\ O & C \end{pmatrix} \begin{pmatrix} M_1 & M_3 \\ M_2 & M_4 \end{pmatrix}. \tag{18}
$$

3.4 Properties of the leading-order solution

Here we examine various properties of the leading-order solution defined by (15) and (16).

3.4.1 Inner and outer layers

Up to terms of order ε the leading-order solution can be put into various equivalent forms. In the inner layer defined by $t \leq O(\varepsilon)$ the leading-order solution is equivalent to

$$
\begin{aligned}
&\eta(t) = \eta_0, \\
&\left\{ \begin{array}{c} p(t) \\ \pi(t) \end{array} \right\} = \exp(-At/\varepsilon) \left\{ \begin{array}{c} p_0 \\ \pi_0 \end{array} \right\} + [I - \exp(-At/\varepsilon)]A^{-1} \left\{ \begin{array}{c} \eta_0 \\ 0 \end{array} \right\}.
\end{aligned} \tag{19}
$$

In contrast, in the outer layer defined by $t \geq O(1)$ the leading-order solution is equivalent to

$$
\begin{aligned}
p(t) &= mv(t) = mM_1\eta(t), \\
\pi(t) &= C\omega(t) = CM_2\eta(t),
\end{aligned} \tag{20}
$$

where $\eta(t)$ satisfies (16). This outer solution will be exploited later when we consider the notion of sedimentation speed.

3.4.2 General structure

The leading-order equation (16) has the structure of the classic Euler equation of rigid body mechanics with $M_2 \in \mathbb{R}^{3\times 3}$ playing the role of the inertia matrix. However, in contrast to the classic case, the mobility matrix M_2 need not be symmetric. Here we discuss several features of the dynamics defined by this generalized Euler equation.

Basic integral. Regardless of the specific form of M_2 we find that (16) possesses the integral

$$F_1(\eta) = |\eta|^2. \tag{21}$$

In particular, any solution of (16) evolves on a sphere defined by $F_1 = |\eta_0|^2$. This is a consequence of the fact that η are the components in a moving frame of a constant vector $\boldsymbol{\eta}$. Moreover, our choice of non-dimensionalization implies $|\eta_0| = 1$. Thus all solutions that we consider will evolve on the unit sphere.

Degenerate case. When $M_2 = cI$ ($c \in \mathbb{R}$) the generalized Euler equation takes the trivial form $\dot{\eta} = 0$. Thus all solutions are constant in this case.

Symmetric case. When $M_2^T = M_2$ ($M_2 \neq cI,\ c \in \mathbb{R}$) the generalized Euler equation possesses a second independent integral given by

$$F_2(\eta) = \eta \cdot M_2\eta. \tag{22}$$

Thus any solution of (16) evolves in the intersection of the unit sphere $F_1 = 1$ and the quadratic surface $F_2 = c_2$, where c_2 is a constant determined by the initial value of η. In this symmetric case notice that (16) can be written in the non-canonical Hamiltonian form

$$\dot{\eta} = J(\eta)\nabla H(\eta), \tag{23}$$

with Hamiltonian $H(\eta) = \frac{1}{2}\eta \cdot M_2\eta$ and structure matrix $J(\eta) = [\eta\times]$. Here $[\eta\times] \in \mathbb{R}^{3\times 3}$ is the skew-symmetric matrix defined by the coordinate vector η via

$$[\eta\times] = \begin{pmatrix} 0 & -\eta_3 & \eta_2 \\ \eta_3 & 0 & -\eta_1 \\ -\eta_2 & \eta_1 & 0 \end{pmatrix}. \tag{24}$$

For more details on the theory of such systems see, for example, [11].

Skew case. When $M_2^T = -M_2$ ($M_2 \neq 0$) the generalized Euler equation can be interpreted as the projection of a constant vector field onto a sphere. In particular, if we let $m_2 \in \mathbb{R}^3$ denote the unique axial vector of M_2 defined such that $[m_2\times] = M_2$, then we find that (16) can be written in the form

$$\dot{\eta} = \eta \times ([m_2\times]\eta) = \eta \times (m_2 \times \eta) = |\eta|^2 m_2 - (\eta \cdot m_2)\eta, \tag{25}$$

where the last equality follows from the vector identity $x \times (y \times z) = (x \cdot z)y - (x \cdot y)z$. When restricted to the sphere $F_1 = 1$ the vector field in (25) is just the projection of m_2 onto each tangent plane. Notice that any solution curve of (25) has the property that $\dot{\eta}$, η and m_2 are all coplanar. Since any plane through the origin containing m_2 intersects the sphere $F_1 = 1$ in a great circle through the antipodal points $\pm m_2/|m_2|$, we deduce that any solution curve of (25) must lie on the arc of such a circle. We note that along solutions of (25) the function $g(\eta) = m_2 \cdot \eta$ satisfies $|g| \leq |m_2|$ and $\dot{g} = |m_2|^2 - g^2$. Thus g is a Lyapunov function that can be exploited to deduce analytically that the steady state $\eta = m_2/|m_2|$ is globally asymptotically stable (in the sense that it is the limit of all solutions except the unstable steady state $\eta = -m_2/|m_2|$).

General case. When M_2 is neither symmetric nor skew-symmetric an explicit geometrical characterization of solution curves is unavailable. Nevertheless, we shall demonstrate that for all M_2 that are generic in an appropriate sense, the dynamics can be understood as a deformation of either the skew or symmetric case depending on whether M_2 has one or three real eigenvalues.

3.4.3 Long-time behavior

The long-time behavior of the leading-order solution is completely determined by that of the generalized Euler equation. Our first result follows from the fact that the matrix $[I - \exp(-At/\varepsilon)]$ is invertible for any $t > 0$:

Proposition 3.1 *The triple (η_0, p_0, π_0) is a steady state of (15) and (16) if and only if $p_0 = mM_1\eta_0$, $\pi_0 = CM_2\eta_0$ and η_0 is a steady state of (16).*

Thus the steady states of the leading-order dynamics are completely determined by those of (16).

The next result follows from (15) and the fact that $\exp(-At/\varepsilon)$ tends to the zero matrix as $t \to \infty$:

Proposition 3.2 *Let (η_a, p_a, π_a) $(a = 1, 2)$ be any two solutions of (15) and (16). Then for any $\delta > 0$ there is a $T_\delta > 0$ such that*

$$||\Delta\eta||_3 \leq |||(\Delta\eta, \Delta p, \Delta\pi)||| \leq \beta||\Delta\eta||_3 + \delta, \quad \forall t > T_\delta, \tag{26}$$

where $\Delta(\cdot) = (\cdot)_2 - (\cdot)_1$ and $\beta > 1$ is a fixed constant depending only on the parameters m, C, M_1 and M_2. Here $||\cdot||_n$ is the standard Euclidean norm on $\mathbb{R}^n$ and $|||\cdot|||$ is a norm on $\mathbb{R}^9$ defined as $|||(\eta, p, \pi)||| = ||\eta||_3 + ||(p, \pi)||_6$.

Thus the stability of a leading-order steady state is also completely determined by that of (16).

4 Steady states and stability

Here we characterize all possible steady (constant) states of the leading-order dynamics in (15) and (16). We describe the physical rigid body motion associated with each type of steady state and provide criteria that characterize their stability. For convenience we work with the variables (η, v, ω) rather than (η, p, π), where $p = mv$ and $\pi = C\omega$. Recall that all variables are non-dimensional and that any solution of (16) evolves on the unit sphere so that $|\eta| = 1$.

4.1 Characterization of steady states

From Proposition 3.1 and (16) we find that any steady state (η, v, ω) must satisfy the equations

$$\eta \times M_2\eta = 0, \quad v = M_1\eta, \quad \omega = M_2\eta. \tag{27}$$

Since $|\eta| = 1$ we find that $(27)_1$ is satisfied if and only if

$$M_2\eta = \lambda\eta, \qquad \lambda \in \mathbb{R}.$$

Thus, steady states are determined by the real eigenvalues and eigenvectors of M_2. Since any matrix $M_2 \in \mathbb{R}^{3\times3}$ has either one or three real eigenvalues, we are guaranteed that at least one steady state exists. Moreover, depending on its geometric multiplicity, each distinct real eigenvalue of M_2 may generate a family of steady states.

The set of steady states corresponding to an eigenvalue may be characterized as follows. Let λ be a real eigenvalue of M_2 with geometric multiplicity n, $1 \leq n \leq 3$, let E_λ be the corresponding n-dimensional subspace of eigenvectors such that

$$M_2\eta = \lambda\eta, \qquad \forall\eta \in E_\lambda,$$

and let S be the standard unit sphere in $\mathbb{R}^3$. Then all possible steady states corresponding to λ are given by

$$(\eta, v, \omega) = (\eta, M_1\eta, \lambda\eta), \qquad \eta \in E_\lambda \cap S.$$

Notice that $E_\lambda \cap S$ consists of two antipodal points when $n = 1$, a great circle when $n = 2$, and the entire sphere S when $n = 3$.

The fact that the body components η of the prescribed hydrostatic load vector $\boldsymbol{\eta}$ are constant in a steady state partially determines the orientation of the associated body frame $\{\boldsymbol{d}_i\}$. The single remaining freedom is a rotation of the frame $\{\boldsymbol{d}_i\}$ about $\boldsymbol{\eta}$. This rotation is in turn determined by the initial orientation of the frame about $\boldsymbol{\eta}$, and thereafter by the steady-state angular velocity vector $\boldsymbol{\omega}$, whose body components are $\omega = \lambda\eta$. Similarly, the location of the body center of mass is determined by the initial choice, and thereafter by the steady-state linear velocity vector $\boldsymbol{v}$, whose body components are $v = M_1\eta$.

4.2 The four possible types of steady states

The steady state defined by a pair (λ, η) where λ is a real eigenvalue of M_2 and $\eta \in E_\lambda \cap S$ can be one of four possible types.

Vertical translation. In this case (λ, η) satisfies

$$\lambda = 0, \qquad M_1\eta = c\eta \quad (c \in \mathbb{R}),$$

so that η is also a real eigenvector of M_1, and the steady state is

$$(\eta, v, \omega) = (\eta, c\eta, 0).$$

Since the angular velocity vector satisfies $\boldsymbol{\omega} = \sum_i \omega_i \boldsymbol{d}_i = \mathbf{0}$ we deduce that the body frame vectors $\{\boldsymbol{d}_i\}$ are time-independent. Moreover, we deduce that $\boldsymbol{v} = c\boldsymbol{\eta} \neq \mathbf{0}$ (constant), which implies that the body mass center moves with a constant velocity $\boldsymbol{v}$ parallel to $\boldsymbol{\eta}$. The conclusion that $\boldsymbol{v} \neq \mathbf{0}$ follows from the fact that $c = \eta \cdot M_1\eta > 0$ since M_1 is positive-definite.

Non-vertical translation. In this case (λ, η) satisfies

$$\lambda = 0, \qquad M_1\eta \neq c\eta \quad (c \in \mathbb{R}),$$

and the steady state is

$$(\eta, v, \omega) = (\eta, M_1\eta, 0).$$

This implies that the body frame vectors $\{\boldsymbol{d}_i\}$ are constant as before. From the relation $\boldsymbol{v} = \sum_i v_i \boldsymbol{d}_i$ we find that $\boldsymbol{v}$ is also constant, but now $\boldsymbol{v} \neq c\boldsymbol{\eta}$. Thus the velocity of the mass center and the resultant hydrostatic force vector are non-parallel. Nevertheless, we have $\boldsymbol{v} \cdot \boldsymbol{\eta} = \eta \cdot M_1\eta > 0$ due to the definiteness of M_1.

Vertical spin. In this case (λ, η) satisfies

$$\lambda \neq 0, \qquad M_1 \eta = c\eta \quad (c \in \mathbb{R}),$$

and the steady state is

$$(\eta, v, \omega) = (\eta, c\eta, \lambda\eta).$$

Here the angular velocity vector satisfies $\boldsymbol{\omega} = \lambda\boldsymbol{\eta}$ (constant), which implies that the body frame vectors $\{\boldsymbol{d}_i\}$ undergo a steady rotation about the fixed axis $\boldsymbol{\eta}$. The rotation is right-handed about $\boldsymbol{\eta}$ when $\lambda > 0$, and left-handed when $\lambda < 0$. The linear velocity vector satisfies $\boldsymbol{v} = c\boldsymbol{\eta}$ (constant), which implies that the body mass center moves with a constant velocity in the direction of $\boldsymbol{\eta}$ since c is necessarily positive.

Helical spin. In this case (λ, η) satisfies

$$\lambda \neq 0, \qquad M_1 \eta \neq c\eta \quad (c \in \mathbb{R}),$$

and the steady state is

$$(\eta, v, \omega) = (\eta, M_1\eta, \lambda\eta).$$

Again we find that the angular velocity vector satisfies $\boldsymbol{\omega} = \lambda\boldsymbol{\eta}$ (constant), which implies that the body frame vectors $\{\boldsymbol{d}_i\}$ undergo a steady rotation about the fixed axis $\boldsymbol{\eta}$, with the handedness of the rotation determined by the sign of λ. While $\boldsymbol{v}$ and $\boldsymbol{\eta}$ are non-parallel we find that $\boldsymbol{v} \cdot \boldsymbol{\eta} = \eta \cdot M_1\eta > 0$ (constant) as before.

The body center of mass traces out a helical path. The axis of this path is parallel to $\boldsymbol{\eta}$, and the radius ρ and pitch ν are given by

$$\rho = \frac{|\eta \times M_1\eta|}{|\lambda|} \quad \text{and} \quad \nu = 2\pi\,\frac{\eta \cdot M_1\eta}{|\lambda|}. \tag{28}$$

These conclusions may be reached by decomposing $\boldsymbol{v}$ into parts parallel and perpendicular to the rotation axis $\boldsymbol{\eta}$. In particular, using the fact that $v = M_1\eta$ and $|\boldsymbol{\eta}| = 1$ we have

$$\boldsymbol{v} = (\boldsymbol{v} \cdot \boldsymbol{\eta})\boldsymbol{\eta} + \boldsymbol{v}^{\perp} = (\eta \cdot M_1\eta)\boldsymbol{\eta} + \boldsymbol{v}^{\perp} \tag{29}$$

where $\boldsymbol{v}^{\perp}$ is the projection of $\boldsymbol{v}$ perpendicular to $\boldsymbol{\eta}$. Since $\boldsymbol{v}^{\perp}$ is perpendicular to $\boldsymbol{\omega} = \lambda\boldsymbol{\eta}$ there is a unique vector $\boldsymbol{q}$, also perpendicular to $\boldsymbol{\omega}$, such that

$$\boldsymbol{v}^{\perp} = \boldsymbol{\omega} \times \boldsymbol{q}. \tag{30}$$

In particular, by taking the cross product of (30) with $\boldsymbol{\omega}$ we obtain

$$\boldsymbol{q} = \frac{\boldsymbol{v}^{\perp} \times \boldsymbol{\omega}}{|\boldsymbol{\omega}|^2} = \frac{\boldsymbol{v} \times \boldsymbol{\omega}}{|\boldsymbol{\omega}|^2}. \tag{31}$$

From (31) we deduce that the components of $\boldsymbol{q}$ in the body frame $\{\boldsymbol{d}_i\}$ are constant because $\boldsymbol{v}$ and $\boldsymbol{\omega}$ have constant components in this frame. Thus $\boldsymbol{q}$ is fixed in, and rotating with, the body and we find that

$$\dot{\boldsymbol{q}} = \boldsymbol{\omega} \times \boldsymbol{q}. \tag{32}$$

Substitution of (32) and (30) into (29) then yields

$$\boldsymbol{v} = (\eta \cdot M_1 \eta)\boldsymbol{\eta} + \dot{\boldsymbol{q}}. \tag{33}$$

In view of the fact that $\dot{\boldsymbol{r}} = \boldsymbol{v}$ we obtain

$$\boldsymbol{r}(t) = \boldsymbol{b} + t(\eta \cdot M_1 \eta)\boldsymbol{\eta} + \boldsymbol{q}(t), \tag{34}$$

where $\boldsymbol{b}$ is a constant of integration. Since $\boldsymbol{q}$ is perpendicular to $\boldsymbol{\eta}$ and rotates around this vector with a steady angular velocity we deduce that $\boldsymbol{r}$ traces out a helix. The axis of this helix is parallel to $\boldsymbol{\eta}$ and passes through the point $\boldsymbol{b}$ (determined by initial conditions). The radius ρ of the helix is determined by the magnitude of $\boldsymbol{q}$; in particular, $\rho = |\boldsymbol{q}|$. This relation together with (31) leads to the expression in $(28)_1$. Finally, the pitch ν of the helix is determined by the angular velocity $\boldsymbol{\omega}$ and the projection of the linear velocity $\boldsymbol{v}$ onto the helix axis $\boldsymbol{\eta}$; in particular, $\nu = 2\pi|\boldsymbol{v} \cdot \boldsymbol{\eta}|/|\boldsymbol{\omega}|$. This relation leads to the expression in $(28)_2$.

From (28) and the elementary geometry of a helix with curvature κ and torsion τ we have

$$\frac{\kappa}{|\tau|} = \frac{2\pi\rho}{\nu} = \frac{|\eta \times M_1 \eta|}{\eta \cdot M_1 \eta} = \tan\psi, \tag{35}$$

where $0 \le \psi < \pi/2$ is the angle between the helix axis and unit tangent vector. Thus the value of $\tan\psi$ determines the aspect ratio of the helix, the ratio $|M_1\eta|/|M_2\eta| = |M_1\eta|/|\lambda|$ determines the scale via (28), and the handedness is determined by the sign of the eigenvalue λ.

4.3 Stability results for generic bodies

In this section we demonstrate that a rather complete stability analysis of the steady motions can be carried out, largely independent of the details of the mobility matrices. For simplicity we exclude consideration of the case of $M_2 \in \mathbb{R}^{3\times 3}$ having multiple eigenvalues, because then many subcases arise. Of necessity we exclude certain other cases, such as M_2 being symmetric, in which a certain off-diagonal entry in the Schur form of M_2 vanishes, for then our conclusions are not valid. To this end we define a rigid body to be *generic* when its associated mobility matrix $M_2 \in \mathbb{R}^{3\times 3}$ defined in (10) satisfies one of two conditions:

(G1) M_2 has one real eigenvalue, and a genuinely complex conjugate pair of eigenvalues.

(G2) M_2 has three, distinct, real eigenvalues, and the corresponding normalized eigenvectors η_k satisfy

$$\eta_i \cdot \eta_j \neq (\eta_i \cdot \eta_k)(\eta_j \cdot \eta_k) \quad (i, j, k \text{ distinct}), \tag{36}$$

for values of the index k corresponding to the maximum and minimum eigenvalues.

Because (36) is symmetric in the indices i and j, we obtain one independent condition on the eigenvectors for each value of k corresponding to an extreme eigenvalue. These genericity conditions will play a role in the construction of Lyapunov functions. We remark that condition (36) fails whenever M_2 is symmetric, for then eigenvectors corresponding to distinct eigenvalues are necessarily orthogonal. Moreover, a simple analysis of condition (36) shows that it can fail for other exceptional, non-symmetric matrices. For example, if η_i and η_j are regarded as prescribed, then (36) fails whenever η_k lies in the surface of a certain cone.

Our main stability result is:

Theorem 4.1 *Consider a rigid body with hydrodynamic mobility matrix M_2 as defined in (10).*

1. *If M_2 satisfies the genericity condition (G1) with the real eigenvalue λ and associated unit eigenvector η, then there are two distinct steady states corresponding to the pair $\pm\eta$. One of these states is globally asymptotically stable, and the other is unstable.*

2. *If M_2 satisfies the genericity condition (G2) and the three distinct real eigenvalues are ordered as $\lambda_A < \lambda_B < \lambda_C$ with associated unit eigenvectors $\{\eta_A, \eta_B, \eta_C\}$, then there are six distinct steady states corresponding to the pairs $\{\pm\eta_A, \pm\eta_B, \pm\eta_C\}$. Both states in the middle pair $\pm\eta_B$ are unstable. The pairs $\pm\eta_A$ and $\pm\eta_C$ each contain one asymptotically stable, and one unstable state.*

Thus every generic body has either two or six different steady states depending on whether M_2 has one or three real eigenvalues. In the first case one state is stable and the other is unstable. The stable state has the property that it is the limit of all motions except for the unstable state, and for this reason we refer to it as being globally asymptotically stable. In the second case two are stable, and four are unstable, with both of the stable states being locally, asymptotically stable.

Our genericity assumptions exclude the case when M_2 is symmetric. However, in this (classic) case the stability properties of the Euler equation (16) are well-known. For example, when M_2 is symmetric and has three distinct eigenvalues there are six different steady states. Just as in the generic case, the two steady states corresponding to the middle eigenvalue are both unstable. However, in contrast to the generic case, the two steady states corresponding to each extremum eigenvalue are both stable, but not asymptotically stable.

Cases (1) and (2) of Theorem 4.1 can be understood as deformations of the two extreme cases of M_2 being, respectively, either exactly skew-symmetric or exactly symmetric. When M_2 satisfies (G1), the simple vector field described in Section 3.4.2 with a single, globally asymptotically stable node may either remain unaltered or be twisted into a vector field with a single, globally asymptotically stable spiral. When M_2 satisfies (G2), the Hamiltonian vector field with two saddles and four centers is deformed into a vector field with two saddles and four spirals, two asymptotically stable and two unstable. Note that when M_2 satisfies (G2) we have reached no conclusion regarding the possible persistence under deformation of some of the periodic orbits arising in the Hamiltonian case.

For purposes of comparison we develop our stability results for the generalized Euler equation (16) in three parts. In the first part we present a linear stability analysis that applies in both cases (1) and (2) above. Based on insights gained from this analysis, we then construct Lyapunov functions for each case separately and thereby establish the non-linear stability results of Theorem 4.1.

4.3.1 Linear stability

Let (λ_0, η_0) be a real eigenpair of M_2 and consider the generalized Euler equation (16) with an initial condition close to the steady state η_0, that is,

$$\begin{aligned} \dot{\eta} &= \eta \times M_2 \eta, \\ \eta(0) &= \eta_0 + \delta\phi, \end{aligned} \tag{37}$$

where $\delta\phi$ is a given perturbation. Here $0 \leq \delta \ll |\eta_0| = 1$ specifies the size of the perturbation, and $\phi \in \mathbb{R}^3$, $|\phi| = 1$, specifies the direction. Supposing that the solution $\eta(t)$ can be expanded in powers of δ as

$$\eta(t) = \eta_0 + \delta\gamma(t) + \delta^2\nu(t) + \cdots, \tag{38}$$

our goal is to determine the behavior of the first-order correction term $\gamma(t)$ for an arbitrary perturbation direction ϕ. In accordance with standard definitions, we will say that η_0 is linearly stable if

$$|\gamma(t)| \leq \text{const}, \quad \forall t \geq 0, \quad \forall \phi.$$

Otherwise, we will say that η_0 is unstable.

Linear stability as an eigenvalue problem. To determine an equation for $\gamma(t)$ we substitute the expansion (38) into (37). Collecting coefficients in powers of δ leads to the linear equation

$$\begin{aligned} \dot{\gamma} &= \Gamma(\lambda_0, \eta_0)\gamma, \\ \gamma(0) &= \phi, \end{aligned} \tag{39}$$

where $\Gamma(\lambda_0, \eta_0) \in \mathbb{R}^{3\times 3}$ is a constant matrix defined as

$$\Gamma(\lambda_0, \eta_0) = [\eta_0 \times](M_2 - \lambda_0 I). \tag{40}$$

Thus the linear stability of a particular steady state η_0 is determined by the eigenvalues and Jordan structure of $\Gamma(\lambda_0, \eta_0)$. Since $\Gamma(\lambda_0, -\eta_0) = -\Gamma(\lambda_0, \eta_0)$ we notice that the stability properties of the steady state pair $\pm\eta_0$ are determined simultaneously.

Analysis of the eigenvalue problem. Let e and n be fixed unit vectors chosen such that $\{\pm\eta_0, e, n\}$ is an orthonormal basis for $\mathbb{R}^3$. Let $Q(\eta_0) \in \mathbb{R}^{3\times 3}$ be the orthogonal matrix defined in column form by $Q = (\eta_0, e, n)$ and consider the change of variable $y = Q^T\gamma$. Then from (39) we find that $y(t)$ satisfies the equation

$$\dot{y}_1 = 0, \qquad \left\{ \begin{array}{c} \dot{y}_2 \\ \dot{y}_3 \end{array} \right\} = J(\eta_0)K(\lambda_0) \left\{ \begin{array}{c} y_2 \\ y_3 \end{array} \right\}, \tag{41}$$

where $J, K \in \mathbb{R}^{2\times 2}$ are defined as

$$J = [\det Q] \begin{pmatrix} 0 & -1 \\ 1 & 0 \end{pmatrix}, \qquad K = \begin{pmatrix} e^T \\ n^T \end{pmatrix} [M_2 - \lambda_0 I]\,(e, n). \tag{42}$$

Furthermore, denoting the eigenvalues of M_2 by λ_0, λ_1 and λ_2, we find that the eigenvalues of K are given by $\alpha_1 = \lambda_1 - \lambda_0$ and $\alpha_2 = \lambda_2 - \lambda_0$. Thus the linear stability of the steady state pair $\pm\eta_0$ is completely determined by the reduced matrix $G = JK \in \mathbb{R}^{2\times 2}$.

The location in the complex plane of the eigenvalues of G can be explicitly determined from the entries of K. In particular, let

$$K = \begin{pmatrix} a & b \\ c & d \end{pmatrix} \quad \text{so that} \quad G = JK = [\det Q] \begin{pmatrix} -c & -d \\ a & b \end{pmatrix}. \tag{43}$$

Then the eigenvalues ξ_1 and ξ_2 of G are given by

$$\xi_{1,2} = [\det Q]\frac{-q \pm \sqrt{q^2 - 4p}}{2}, \tag{44}$$

where $q = c - b \in \mathbb{R}$ and

$$p = \det[K] = \alpha_1\alpha_2 = (\lambda_1 - \lambda_0)(\lambda_2 - \lambda_0) \in \mathbb{R}. \tag{45}$$

A straightforward analysis of (44) yields the following results:

(1) $p < 0 \quad \Rightarrow \quad \xi_{1,2}$ are real, non-zero and of opposite sign.

$(2)_a$ $p > 0$, $q \neq 0$ $\Rightarrow$ $\xi_{1,2}$ are complex with equal, non-zero real parts.

$(2)_b$ $p > 0$, $q = 0$ $\Rightarrow$ $\xi_{1,2}$ are imaginary and distinct.

$(3)_a$ $p = 0$, $q \neq 0$ $\Rightarrow$ $\xi_{1,2}$ are real, distinct and of the same sign.

$(3)_b$ $p = 0$, $q = 0$ $\Rightarrow$ $\xi_{1,2}$ are both zero.

The linear stability of the steady state pair $\pm\eta_0$ can now be characterized in terms of p and q and the fact that $\det Q(-\eta_0) = -\det Q(\eta_0)$. In case (1) we find that both steady states from the pair $\pm\eta_0$ are unstable. In case $(2)_a$ we find that one state in the pair must be stable and the other unstable, whereas in $(2)_b$ both states are neutrally stable. Thus in case (2) there is always at least one linearly stable state in the pair $\pm\eta_0$. In case $(3)_a$ we obtain the same stability results as in $(2)_a$. However, case $(3)_b$ is indeterminate; in particular, linear stability cannot be assessed based solely upon p and q.

Linear stability in the case of one real eigenvalue. Suppose M_2 has only one real eigenvalue λ_A with associated unit eigenvector η_A. The stability matrix $G(\lambda_A, \eta_A)$ has eigenvalues characterized by $p_A = (\lambda_B - \lambda_A)(\lambda_C - \lambda_A)$; moreover, since $\lambda_C = \overline{\lambda_B}$, we have $p_A = |\lambda_B - \lambda_A|^2 > 0$. From (44) we then deduce that in case $(2)_a$ one state in the pair $\pm\eta_A$ is linearly stable and the other unstable, or in case $(2)_b$ both are neutrally stable. However, the case of neutral linear stability will be shown to become asymptotic stability in the non-linear analysis outlined below.

Linear stability in the case of three real eigenvalues. Suppose M_2 has three real eigenvalues $\lambda_A < \lambda_B < \lambda_C$ with associated unit eigenvectors $\{\eta_A, \eta_B, \eta_C\}$. For the minimum eigenvalue λ_A we find that the stability matrix $G(\lambda_A, \eta_A)$ has eigenvalues characterized by $p_A = (\lambda_B - \lambda_A)(\lambda_C - \lambda_A) > 0$. From (44) we then deduce that one state in the pair $\pm\eta_A$ is linearly stable and the other unstable, or both are neutrally stable. The same conclusion holds for the maximum eigenvalue λ_C and the pair $\pm\eta_C$. However, the case of neutral linear stability for each of the extremum eigenvalues is again excluded by the non-linear analysis below. For the middle eigenvalue λ_B we find that the stability matrix $G(\lambda_B, \eta_B)$ has eigenvalues characterized by $p_B = (\lambda_A - \lambda_B)(\lambda_C - \lambda_B) < 0$, which implies that both states in the pair $\pm\eta_B$ are unstable.

4.3.2 Non-linear stability: one real eigenvalue

Suppose M_2 has one real and two complex conjugate eigenvalues denoted by λ_0 and $\lambda_{1,2} = \alpha \pm i\beta$ $(\beta > 0)$, and let η_0 be the unit eigenvector associated with λ_0. To establish case (1) of Theorem 4.1 we will show that

$$g(\eta) = \eta_0 \cdot \eta \tag{46}$$

is a Lyapunov function for the generalized Euler equation (16).

To begin, notice that $g \in [-1, 1]$ since η evolves on the unit sphere and that $g = \pm 1$ only when $\eta = \pm\eta_0$. Moreover, note that the rate of change of $g(\eta)$ along any solution of (16) is given by

$$\dot{g} = \eta_0 \cdot \dot{\eta} = -\eta \cdot [\eta_0 \times] M_2 \eta, \tag{47}$$

where $[\eta_0 \times]$ is the skew matrix defined according to the rule in (24); in particular, $[\eta_0 \times] v = \eta_0 \times v$ for any $v \in \mathbb{R}^3$.

Just as in Section 4.3.1, let e and n be fixed unit vectors chosen such that $\{\pm\eta_0, e, n\}$ is an orthonormal basis for $\mathbb{R}^3$ and consider the change of variable $y = Q^T \eta$ where $Q(\eta_0) \in \mathbb{R}^{3\times 3}$ is an orthogonal matrix defined in column form by $Q = (\eta_0, e, n)$. Making the substitution $\eta = Qy$ in (47) gives

$$\dot{g} = \left\{ \begin{array}{c} y_2 \\ y_3 \end{array} \right\} \cdot JD \left\{ \begin{array}{c} y_2 \\ y_3 \end{array} \right\}, \tag{48}$$

where $J, D \in \mathbb{R}^{2\times 2}$ are defined as

$$J = [\det Q] \begin{pmatrix} 0 & -1 \\ 1 & 0 \end{pmatrix}, \qquad D = \begin{pmatrix} e^T \\ n^T \end{pmatrix} M_2 \, (e, n). \tag{49}$$

From the definition of Q we have $\det Q = \pm 1$ and $\det Q(-\eta_0) = -\det Q(\eta_0)$. Moreover, since e and n are orthogonal to η_0 we deduce that the two eigenvalues of D must be the two complex conjugate eigenvalues of M_2.

By rotating e and n if necessary, we may put D into the convenient form

$$D = \begin{pmatrix} a & b \\ c & a \end{pmatrix}. \tag{50}$$

In terms of a, b and c the eigenvalues of D are given by $\alpha_{1,2} = a \pm \sqrt{bc}$. Thus we necessarily have $bc < 0$ since $\alpha_{1,2}$ must be complex. Without loss of generality we may assume that $b > 0$ and $c < 0$. This can always be achieved by changing the sign of either e or n. Notice that this sign convention for b and c determines a definite sign for $\det Q(\eta_0)$.

The fact that g is a Lyapunov function can now be established. By expanding the quadratic form in (48) we find that

$$\dot{g} = \det Q\{-cy_2^2 + by_3^2\} = \det Q\{|c|(\eta \cdot e)^2 + |b|(\eta \cdot n)^2\}, \tag{51}$$

where the last line follows from $y = Q^T\eta$ and the sign convention on b and c. In the case when $\det Q(\eta_0) = 1$ we have

$$\dot{g} = |c|(\eta \cdot e)^2 + |b|(\eta \cdot n)^2 \geq \kappa[1 - g^2], \tag{52}$$

where $\kappa = \min\{|b|, |c|\} > 0$. Since $g \in [-1, 1]$ we have $\kappa[1 - g^2] \geq 0$. Moreover, $\kappa[1 - g^2] > 0$ for all $g \in (-1, 1)$. With the exception of the two distinct steady states $\pm\eta_0$ which correspond to the points $g = \pm 1$, we find that all solutions η of (16) have the property that $\dot{g} > 0$. Thus g must tend to unity along these solutions and we conclude that η_0 is globally asymptotically stable, and, by necessity, $-\eta_0$ is unstable. A similar argument can be used when $\det Q(\eta_0) = -1$. In this case we conclude that $-\eta_0$ is globally asymptotically stable whereas η_0 is unstable.

4.3.3 Non-linear stability: three real eigenvalues

The non-linear analysis outlined above does not carry over to the case when M_2 has three real eigenvalues λ_k ($k = 0, 1, 2$) with corresponding unit eigenvectors η_k. In this case the matrix D defined in (49) must have two real eigenvalues, and from (50) we deduce that $bc > 0$. This implies that the quadratic form in (48) is necessarily indefinite and g is no longer a Lyapunov function.

To establish case (2) of Theorem 4.1 we consider a different functional form for g, namely

$$g(\eta) = \tfrac{1}{2}\eta \cdot QSQ^T\eta, \tag{53}$$

where

$$S = \begin{pmatrix} 0 & 0 & 0 \\ 0 & v & \gamma \\ 0 & \gamma & w \end{pmatrix}, \tag{54}$$

$v = \lambda_1 - \lambda_0$, $w = \lambda_2 - \lambda_0$, Q is a certain orthogonal matrix and $\gamma > 0$ is a sufficiently small constant. Using this function we will establish the results for the case when λ_0 is an extremum eigenvalue. The non-linear instability results for the case when λ_0 is the middle eigenvalue follow directly from the linear analysis given above [6].

To begin, let e and n be fixed unit vectors chosen such that

$$Q^T M_2 Q = \begin{pmatrix} \lambda_0 & a & b \\ 0 & \lambda_1 & c \\ 0 & 0 & \lambda_2 \end{pmatrix}, \tag{55}$$

where $Q(\eta_0) \in \mathbb{R}^{3\times 3}$ is an orthogonal matrix defined in column form by $Q = (\eta_0, e, n)$ and a, b and c are constants. This is always possible by the Schur decomposition theorem for matrices with real eigenvalues. A straightforward calculation shows that the genericity condition (36) on the eigenvectors η_k is a necessary and sufficient condition that $c \neq 0$. Moreover, without loss of generality we may assume $c > 0$. This can always be achieved by changing the sign of e if necessary. Notice that this sign convention for c determines a definite sign for $\det Q(\eta_0)$.

In terms of the variable $y = Q^T \eta$ the steady-state pair $\eta = \pm\eta_0$ becomes $y = \pm(1, 0, 0)$. Moreover, we obtain

$$g = \tfrac{1}{2} y \cdot Sy, \tag{56}$$

and we find that the rate of change of g along any solution of (16) is given by

$$\dot{g} = [\det Q]\, y_1 \left\{ \begin{array}{c} y_2 \\ y_3 \end{array} \right\} \cdot K \left\{ \begin{array}{c} y_2 \\ y_3 \end{array} \right\} + O(y_2^2 y_3, y_2 y_3^2, y_2^3, y_3^3), \tag{57}$$

where $K \in \mathbb{R}^{2\times 2}$ is defined as

$$K = \begin{pmatrix} v\gamma & c\gamma/2 \\ c\gamma/2 & (c-\gamma)w \end{pmatrix}. \tag{58}$$

The stability results for the case when λ_0 is an extremum eigenvalue can now be established. Supposing λ_0 is the maximum eigenvalue and that the constant γ is chosen such that

$$0 < \gamma < \min\{\frac{4vwc}{4vw + c^2}, \sqrt{vw}\},$$

we find that g has strict local maxima on the unit sphere $|y| = 1$ at the points $y = \pm(1, 0, 0)$. Furthermore, we find that K is negative-definite, which in view of (57) implies that $\dot{g}$ is sign-definite in a sufficiently small neighborhood of each of the points $y = \pm(1, 0, 0)$. When $\det Q(\eta_0) = 1$ we find $\dot{g} > 0$ in a neighborhood of $y = (-1, 0, 0)$ and $\dot{g} < 0$ in a neighborhood of $y = (1, 0, 0)$, which implies that $-\eta_0$ is stable and η_0 is unstable. On the other hand, when $\det Q(\eta_0) = -1$, we find that η_0 is stable and $-\eta_0$ is unstable. Similar arguments can be used when λ_0 is the minimum eigenvalue. In this case g has strict local minima on the unit sphere $|y| = 1$ at the points $y = \pm(1, 0, 0)$ and K is positive-definite. As before, we find that $-\eta_0$ is stable and η_0 is unstable when $\det Q(\eta_0) = 1$, and that η_0 is stable and $-\eta_0$ is unstable when $\det Q(\eta_0) = -1$.

5 Sedimentation speed

Dependent upon the shape of a rigid body as expressed in the mobility matrices M_1 and M_2, the leading-order dynamics in (15) and (16) show that the body may admit a range of different unsteady motions, together with a number of different steady states. We define the *sedimentation speed* ϑ of any such motion to be the component of the body mass center velocity $\boldsymbol{v} = \sum_i v_i \boldsymbol{d}_i$ in the direction of the (constant) hydrostatic load $\boldsymbol{\eta} = \sum_i \eta_i \boldsymbol{d}_i$. In particular, using the fact that $|\eta| = 1$ we have

$$\vartheta = v \cdot \eta. \tag{59}$$

Here we exploit our perturbation results to characterize how the sedimentation speed ϑ depends on the shape of a body.

5.1 Upper and lower bounds

For times $t \geq O(1)$ the outer layer solution (20) shows that to leading order

$$v = M_1 \eta,$$

where $M_1 \in \mathbb{R}^{3\times 3}$ is the symmetric, positive-definite mobility matrix defined in (10). Substituting this result into (59) we find that

$$\vartheta = \eta \cdot M_1 \eta, \quad t \geq O(1). \tag{60}$$

Denoting the eigenvalues of M_1 by $\theta_{\max} \geq \theta_{\mathrm{mid}} \geq \theta_{\min} > 0$ we conclude that ϑ is bounded above and below as

$$\theta_{\min} \leq \vartheta \leq \theta_{\max}, \quad t \geq O(1). \tag{61}$$

Notice that these bounds apply regardless if the body motion is steady or not.

5.2 Characteristic value

Except for the case when a body possesses a steady state that is globally asymptotically stable, the value of the sedimentation speed will in general depend on the initial conditions of the motion. For example, different initial conditions may lead to different steady states, or possibly even to motions that are not steady. For this reason it is desirable to introduce a characteristic speed ϑ_* associated with sedimentation that is independent of the details of the motion and which depends only on the body shape.

One definition of such a characteristic speed is

$$\vartheta_* = \frac{1}{3}(\theta_{\min} + \theta_{\mathrm{mid}} + \theta_{\max}) = \frac{1}{3}\operatorname{tr}[M_1]. \tag{62}$$

This expression is obtained by averaging the quadratic form in (60) over the unit sphere with a uniform distribution. Notice that this quantity is an intrinsic property of the shape of a body as measured by the mobility matrix M_1, and can be interpreted as a weighted mean of the bounds in (61).

Different definitions for a characteristic speed can also be considered. For example, rather than average the quadratic form in (60) with respect to the uniform distribution on the unit sphere, we might also consider an average with respect to an asymptotic distribution (if one exists) of the generalized Euler equation (16). For example, in case (1) of Theorem 4.1 the asymptotic distribution is concentrated at the globally attracting, asymptotically stable steady state defined by the single real eigenvector η_0 of the mobility matrix M_2, and the characteristic sedimentation speed would be equal to $\eta_0 \cdot M_1\eta_0$, which necessarily satisfies the bounds in (61). However, to find such distributions in cases where there is more than one asymptotically stable steady state we must typically solve an appropriate partial differential (Louiville) equation [14] and explicit expressions are generally unavailable.

6 Simulations of rigid filaments

We illustrate the theory that we have developed with various numerical simulations of the sedimentation dynamics of rigid filaments whose centerlines approximate the ideal configurations of six different knots [7, 12]. That is, we consider the specific case where the body is a closed, rigid loop formed from a tube of small radius and uniform mass density. Under our Stokes approximation, the hydrodynamics of any such body is completely determined by its non-dimensional mass m (which by convention is unity), inertia matrix $C \in \mathbb{R}^{3\times 3}$ and hydrodynamic resistance matrix $L \in \mathbb{R}^{6\times 6}$. Here we continue to follow the convention set in Section 3 and work only with non-dimensional quantities. In particular, the filament center of mass position $\boldsymbol{r}$, centerline coordinates z_a and radius γ introduced below are all scaled by the body characteristic length l, which we take to be the filament length.

6.1 Hydrodynamic model

The exact evaluation of the hydrodynamic resistance matrix L for a filament would require the solution of the Stokes flow equations in the three-dimensional region of space exterior to the filament. The approach we take is to model the continuous filament as a collection of n identical beads distributed along the filament axis and apply the approximations developed in [13].

Since the filament is assumed to be rigid with mass center $\boldsymbol{r}$ and body frame $\{\boldsymbol{d}_i\}$ $(i = 1, 2, 3)$, the position vector of each bead in the model can be written as

$$\boldsymbol{q}_a = \boldsymbol{r} + \sum_{i=1}^{3} z_a^i \boldsymbol{d}_i, \quad (a = 1, \ldots, n). \tag{63}$$

Here $z_a \in \mathbb{R}^3$ are constant coordinates that define the shape of the filament. Each bead in the model is assumed to be a sphere of radius $\gamma > 0$ with mass

$\nu = 1/n > 0$. In this case the total mass m and inertia matrix C (with respect to the mass center and body frame) are given by

$$m = \sum_{a=1}^{n} \nu = 1, \qquad C = \sum_{a=1}^{n} \nu[|z_a|^2 I - z_a \otimes z_a], \tag{64}$$

where $\otimes$ denotes the vector outer product.

To evaluate the resistance matrix L we note that the Stokes equations are linear, so that the viscous drag force $\boldsymbol{f}_a^{(d)}$ on each bead may be expressed as a linear function of all the particle velocities $\boldsymbol{u}_a$. In terms of components $f_a^{(d)} \in \mathbb{R}^3$ and $u_a \in \mathbb{R}^3$ with respect to the body frame we have

$$f_a^{(d)} = -\sum_{b=1}^{n} A_{ab} u_b, \ (a = 1, \ldots, n) \qquad \text{or} \qquad f^{(d)} = -Au, \tag{65}$$

where $f^{(d)} = (f_a^{(d)}) \in \mathbb{R}^{3n}$, $u = (u_a) \in \mathbb{R}^{3n}$ and $A = (A_{ab}) \in \mathbb{R}^{3n \times 3n}$ is a hydrodynamic interaction matrix determined by the Stokes equations that (due to objectivity) depends only upon the relative positions of the beads.

Here we employ (an appropriate non-dimensional form of) the approximation to the interaction matrix due to Rotne and Prager [13]. In particular, we take $A = D^{-1}$ where $D = (D_{ab}) \in \mathbb{R}^{3n \times 3n}$ is a matrix whose diagonal blocks ($a = b$) are defined by

$$D_{aa} = \frac{1}{6\pi\gamma} I, \tag{66}$$

and off-diagonal blocks ($a \neq b$) are defined by

$$D_{ab} = \begin{cases} D_{ab}^{\text{distinct}} & \text{if } |z_{ab}| \geq 2\gamma, \\ D_{ab}^{\text{overlap}} & \text{if } |z_{ab}| < 2\gamma, \end{cases} \tag{67}$$

where

$$\begin{aligned} D_{ab}^{\text{distinct}} = \frac{1}{8\pi|z_{ab}|^3} \Bigg[& \left(I|z_{ab}|^2 + z_{ab} \otimes z_{ab}\right) \\ & + \frac{2\gamma^2}{|z_{ab}|^2} \left(\frac{1}{3} I |z_{ab}|^2 - z_{ab} \otimes z_{ab}\right) \Bigg], \end{aligned} \tag{68}$$

and

$$D_{ab}^{\text{overlap}} = \frac{1}{6\pi\gamma} \left[\left(1 - \frac{9}{32} \frac{|z_{ab}|}{\gamma}\right) I + \frac{3}{32} \frac{z_{ab} \otimes z_{ab}}{\gamma |z_{ab}|} \right]. \tag{69}$$

Here $z_{ab} = z_b - z_a \in \mathbb{R}^3$ are the body coordinates of bead b relative to bead a.

The rigid body resistance matrix $L \in \mathbb{R}^{6 \times 6}$ can be determined from the bead interaction matrix $A \in \mathbb{R}^{3n \times 3n}$. To begin, notice that the components of the resultant hydrodynamic force and torque (about the mass center) are given by

$$f^{(d)} = \sum_{a=1}^{n} f_a^{(d)} \qquad \text{and} \qquad \tau^{(d)} = \sum_{a=1}^{n} z_a \times f_a^{(d)}, \tag{70}$$

and that the components of the bead velocity may be expressed in terms of the rigid body linear and angular velocities as

$$u_a = v + \omega \times z_a. \tag{71}$$

Substitution of (65) and (71) into (70) then leads to the component version of (6), namely

$$f^{(d)} = -L_1 v - L_3 \omega, \qquad \tau^{(d)} = -L_2 v - L_4 \omega, \tag{72}$$

where

$$\begin{array}{rclrcl} L_1 & = & \sum_{a,b=1}^{n} A_{ab}, & L_3 & = & \sum_{a,b=1}^{n} A_{ab}[z_b\times]^T, \\ L_2 & = & \sum_{a,b=1}^{n} [z_a\times]A_{ab}, & L_4 & = & \sum_{a,b=1}^{n} [z_a\times]A_{ab}[z_b\times]^T. \end{array} \tag{73}$$

6.2 Numerical simulations

The starting point for our simulation of rigid filaments dynamics was raw data for the ideal shapes kindly provided by the authors of [7, 12] in the form of lists of points in three-space. The data for each shape was then splined, resampled and scaled to produce a piecewise linear curve of unit length defined by n uniformly-spaced points. At each of these points we then placed a bead of radius $\gamma = 1/(2n)$ so that each bead was tangential to each of its neighbors as illustrated in Figure 1. Thus we arrived at n identical beads with body coordinates z_a $(a = 1, \ldots, n)$ to be used in the Rotne-Prager formulas (66)–(69).

It is not necessary that a filament be modeled by beads that are mutually tangential. As illustrated in Figures 2(a-c) one could fix the bead radius γ and consider different numbers of beads uniformly distributed along the filament, with overlaps arranged so that the length of the piecewise linear curve through the bead centers remains unity. Once a number n of beads is specified, the body resistance matrix L may be computed according to (73). Figure 2(d) presents a plot of the relative error in L as a function of n, where

$$\text{relative error} = \frac{||L(n) - L_e||}{||L_e||}.$$

Here $||\cdot||$ is the Frobenius norm on $\mathbb{R}^{6\times 6}$ and L_e is the resistance matrix computed with $n = 750$. This plot suggests that the Rotne-Prager approximation of L is well-defined in the continuum limit as $n \to \infty$. In particular, any conclusions drawn from L should eventually become independent of n for sufficiently large n.

In all six of our examples we use the same number $n = 200$ of identical, touching beads of radius $\gamma = 1/400$ along each rigid filament of unit length. For each of the six filaments we then apply the Rotne-Prager theory described in Section 6.1 to obtain the hydrodynamic resistance matrix L, and thereby its inverse, the mobility matrix M. In particular, we obtain the sub-blocks M_2 and M_1, whose eigenvalues and eigenvectors determine the numbers and types of all steady motions according to the analysis developed in Section 4. The actual entries in the matrices depend upon the choice of coordinate frame attached to the body, and so are not recorded here. However, each steady motion of a body is characterized by quantities that are independent of this choice of frame. In particular, each steady (screw) motion is characterized by the corresponding eigenvalue λ of M_2, the radius ρ and pitch ν defined in (28), and the hydrodynamic axis defined by the orientation of the corresponding eigenvector with respect to the body frame.

Table 1 and Figure 3 summarize our results for all six example filaments. For each filament Table 1 presents the three eigenvalues of the M_2 matrix, along with the radius and pitch of the helix that is followed by the center of mass of the body in the two steady motions corresponding to each real eigenvalue. For the ideal 3_1, 4_1, 5_1, 6_1 and 7_1 knots the corresponding M_2 matrices each have three, real, distinct eigenvalues, while the M_2 matrix for the 7_7 configuration has one real eigenvalue and a complex conjugate pair. The hydrodynamic axes defined by the real eigenvectors of the M_2 matrix for each filament are illustrated in Figure 3. In all five cases of there being three real eigenvalues, the corresponding eigenvectors satisfied the genericity condition (36). Thus the stability classification of Theorem 4.1 applies, the six examples falling into one of type (G1) and five of type (G2).

	λ	ρ	ν		λ	ρ	ν
3_1	-0.506	1.09e-3	11.6	4_1	-0.796	2.32e-3	7.61
	-0.495	6.67e-4	11.9		$+0.007$	2.03e-1	931
	$+0.634$	5.86e-4	7.97		$+0.781$	2.29e-3	7.71
5_1	-0.769	1.53e-3	8.22	6_1	-0.896	3.32e-2	7.45
	-0.407	1.37e-1	16.4		$+0.253$	1.40e-1	27.0
	$+0.801$	3.86e-2	7.28		$+0.722$	5.36e-2	9.13
7_1	-0.825	2.27e-2	8.47	7_7	-0.414	2.18e-2	17.3
	-0.470	6.77e-2	15.7		$0.25 + \mathrm{i}\, 0.6$	-	-
	$+0.786$	2.41e-2	8.18		$0.25 - \mathrm{i}\, 0.6$	-	-

Table 1: Eigenvalues λ of the M_2 matrix along with the radius ρ and pitch ν of the corresponding steady screw motion for various different knotted filaments. For comparison note that the overall diameter of the knot in Figure 1(f) is approximately 0.1, and that each of the knots has unit length and is drawn to the same scale.

Our results on the existence, multiplicity and stability of steady states are based on a singular perturbation analysis and may be complemented through a direct numerical simulation of the exact dynamics. For these purposes we assume the non-dimensional parameter ε defined in Section 3 is small, specifically $\varepsilon = 0.01$. In the case of a 7_7 knot, which has an M_2 matrix with a single real eigenvalue, our theory predicts a unique, globally asymptotically stable, steady state. A direct numerical simulation of the dynamics for this knot is presented in Figure 4. In the simulation a set of random orientations of the rigid body frame with vanishing initial velocities is taken as initial conditions, and the time evolution is computed using the exact equations of motion (14) with $\varepsilon = 0.01$. The initial distribution of gravity directions in the body frame is illustrated in panel (b) along with the single hydrodynamic axis of the body. The initial orientations of the body are chosen so as to produce a uniform distribution of gravity directions on the unit sphere. The final distribution of gravity directions in the body frame is shown in panel (c). In concordance with Theorem 4.1 the initial distribution of gravity directions converge to the globally asymptotically stable steady state defined by (one end of) the hydrodynamic axis. Panel (d) shows a plot of sedimentation speed versus time for a few members of the sample. After a thin initial layer in time, which arises because each member begins from rest, the sedimentation speed becomes bounded above and below by the maximum and minimum eigenvalues of M_1 as predicted in (61).

In the case of a 7_1 knot, which has an M_2 matrix with three real, distinct eigenvalues and eigenvectors satisfying our genericity condition, our theory predicts two (locally) asymptotically stable, steady states. A direct numerical simulation of the exact dynamics for this knot using the same procedure and value of ε as before is presented in Figure 5. Notice that the initial distribution of gravity directions illustrated in panel (b) converges to the two asymptotically stable steady states associated with the minimum and maximum eigenvalues as illustrated in panel (c). Our numerical simulation suggests that in this example the two stable states contain the limits of all motions, except the four unstable states. However, this behavior is not guaranteed even in the leading-order dynamics because case (2) of Theorem 4.1 does not preclude the existence of other stable invariant sets such as limit cycles. Any limiting value of the sedimentation speed must nevertheless satisfy the bounds in (61) as illustrated in panel (d).

6.3 Remarks on ideal shapes

The primary purpose of the numerical examples described above is to make concrete the theory developed in this article for arbitrary rigid bodies. Nevertheless, for our examples we have chosen to use rigid filaments approximating the ideal shapes of various knot types. Our choice was motivated by experimental data [16, 17] which revealed an approximate linear relationship between the gel electrophoresis speeds of different (flexible) DNA knots and the average crossing number of their ideal geometrical forms. This observation raises the possibility that ideal shapes may have special hydrodynamic properties. Here we note that our simulations of rigid filaments in a Stokes fluid further suggest that ideal shapes may be hydrodynamically special.

Figure 6 shows plots of sedimentation speed versus average crossing number for the various different ideal knots illustrated in Figure 1(a-f). Two different measures of sedimentation speed are computed for each knot. The first is the average sedimentation speed computed from the numerical simulations outlined in Figures 4 and 5. In particular, for each ideal shape a sample of randomly oriented knots is started from rest and their time evolution is computed until a large final time, at which point the average of the sedimentation speed ϑ over the sample is calculated. In principle, this measure depends on various details of the simulation including the initial distribution of orientations, the initial distribution of linear and angular velocities, and the final time. The second measure is the characteristic sedimentation speed ϑ_* given in (62). As defined, this measure depends only upon the shape of a knot. Both measures reveal an approximate linear relation between sedimentation speed and average crossing number. In particular, rigid filaments of the same length, radius and mass exhibit different sedimentation speeds depending on their knot type.

The steady motions of ideal shapes also exhibit some interesting features. An inspection of Table 1 shows that in no case is a zero eigenvalue achieved, although the 4_1 knot is close to having a zero eigenvalue. Thus each knot spins in each steady state. Furthermore, all the steady motions are genuine screw motions. However, the radii of the helical paths are all small compared to the overall dimensions of the filament, while the pitches are large. Equivalently, the angles ψ defined in (35) are all nearly zero, indicating that the eigenvectors of the M_2 matrices are all close to being eigenvectors of the corresponding M_1 matrices. Moreover, all six examples are generic with one of type (G1) and five of type (G2), although the 3_1 knot is close to having a repeated eigenvalue. (Specifically, the difference between the two sides of the genericity inequalities (36) was of the order 10^{-2}.) While we have not made an extensive study of non-ideal filament shapes, there are some indications that the $1:5$ ratio between the number of cases (G1) and (G2) is in some sense atypical amongst all smooth closed loops.

Figure 3 suggests various symmetries in the shapes of ideal knots. For example, the views of the 3_1, 4_1 and 5_1 knots parallel to their hydrodynamic axes all contain shapes that appear to be symmetric, or close to symmetric in the cases of panels (c) and (k). In contrast, the various views of the 6_1, 7_1 and 7_7 knots contain shapes that are all seemingly non-symmetric. The ideal 4_1 knot appears to have the most symmetry amongst all the examples. In fact, for the 4_1 knot the views along the minimum and maximum hydrodynamic axes shown in panels (f) and (h) contain shapes that appear to be nearly identical up to a rotation. Moreover, the view along the middle axis contains a shape that appears to have four-fold symmetry.

These remarks about the data in Table 1 and Figure 3 highlight the approximate nature of both the input configurations and our numerical simulations. The ideal configurations obtained from [7, 12] are not known analytically, and are based on delicate computations for which error estimates are currently unavailable. Similarly, the Rotne-Prager theory yields only an approximation of the hydrodynamic matrices. Consequently, it is possible that on true ideal shapes the 3_1 knot could have a double eigenvalue, the 4_1 knot could have three eigenvalues of the form $\{0, \pm\lambda\}$, the views along the middle hydrodynamic axes of the 3_1 and 5_1 knots could be closer to symmetric, and some or all of the steady motions could be translations.

7 Generalization to non-uniform bodies

Here we drop the assumption that the centers of mass and volume of the body are coincident. We show that all our previous results on the characterization of steady states, stability and sedimentation speed carry over to the more general case in a straightforward way.

To begin, we return to dimensional variables, and consider an arbitrary rigid body whose center of volume is displaced from the center of mass by the *mass eccentricity vector* $\boldsymbol{\gamma}$. When such a body is immersed in a uniform fluid in the presence of a uniform gravitational field with direction parallel to the unit vertical $\boldsymbol{e}_3$, the net effects of gravitational and hydrostatic (or buoyancy) forces are given by the resultant force and torque

$$\boldsymbol{f}^{(s)} = \boldsymbol{\eta}, \qquad \boldsymbol{\tau}^{(s)} = \boldsymbol{\Delta} \times \boldsymbol{\eta}, \tag{74}$$

where $\boldsymbol{\eta} = \alpha \boldsymbol{e}_3$ and $\boldsymbol{\Delta} = \beta \boldsymbol{\gamma}$ [4]. Here α and β are parameters given by

$$\alpha = (m - m_f)g, \qquad \beta = \frac{m_f}{m_f - m}, \tag{75}$$

where m is the mass of the body, m_f is the mass of the fluid displaced by the body, and g is the gravitational acceleration constant.

When (74) is used in place of (5) we find that the balance laws in (7) now take the form

$$\begin{array}{rcl} \dot{\boldsymbol{\eta}} & = & \boldsymbol{0}, \\ \dot{\boldsymbol{p}} & = & -\boldsymbol{L}_1 \boldsymbol{v} - \boldsymbol{L}_3 \boldsymbol{\omega} + \boldsymbol{\eta}, \\ \dot{\boldsymbol{\pi}} & = & -\boldsymbol{L}_2 \boldsymbol{v} - \boldsymbol{L}_4 \boldsymbol{\omega} + \boldsymbol{\Delta} \times \boldsymbol{\eta}. \end{array} \tag{76}$$

In terms of components with respect to the body frame we find that these equations become

$$\begin{array}{rcl} \dot{\eta} + \omega \times \eta & = & 0, \\ \dot{p} + \omega \times p & = & -L_1 v - L_3 \omega + \eta, \\ \dot{\pi} + \omega \times \pi & = & -L_2 v - L_4 \omega + \Delta \times \eta, \end{array} \tag{77}$$

where $v = m^{-1} p$ and $\omega = C^{-1} \pi$. The hydrodynamic resistance matrices $L_a \in \mathbb{R}^{3\times 3}$ $(a = 1, \dots, 4)$, the inertia matrix $C \in \mathbb{R}^{3\times 3}$ and the (scaled) mass eccentricity vector $\Delta \in \mathbb{R}^3$ are all constant when expressed in the body frame.

When the non-dimensional variables and parameters defined in Section 3 are introduced into (77) we obtain

$$\begin{array}{rcl} \dot{\bar{\eta}} + \bar{\omega} \times \bar{\eta} & = & 0, \\ \varepsilon[\dot{\bar{p}} + \bar{\omega} \times \bar{p}] & = & -\bar{L}_1 \bar{v} - \bar{L}_3 \bar{\omega} + \bar{\eta}, \\ \varepsilon[\dot{\bar{\pi}} + \bar{\omega} \times \bar{\pi}] & = & -\bar{L}_2 \bar{v} - \bar{L}_4 \bar{\omega} + \bar{\Delta} \times \bar{\eta}, \end{array} \tag{78}$$

where $\bar{\Delta} = (1/l)\Delta$, and $\varepsilon = m|\alpha|/\mu^2 l^3$ as before.

Dropping overbars for convenience, we find that a uniform leading-order solution for (78) is given by

$$\left\{ \begin{array}{c} p(t) \\ \pi(t) \end{array} \right\} = \exp(-At/\varepsilon) \left\{ \begin{array}{c} p_0 - mD_1\eta_0 \\ \pi_0 - CD_2\eta_0 \end{array} \right\} + \left\{ \begin{array}{c} mD_1\eta(t) \\ CD_2\eta(t) \end{array} \right\}, \tag{79}$$

where $\eta(t)$ satisfies the initial value problem

$$\begin{aligned} \dot{\eta} &= \eta \times D_2 \eta, \\ \eta(0) &= \eta_0. \end{aligned} \tag{80}$$

Here $A \in \mathbb{R}^{6\times 6}$ is as defined in (17) and the matrices $D_a \in \mathbb{R}^{3\times 3}$ $(a = 1, 2)$ are defined by

$$D_1 = M_1 + M_3[\varDelta\times], \qquad D_2 = M_2 + M_4[\varDelta\times], \tag{81}$$

where $[\varDelta\times] \in \mathbb{R}^{3\times 3}$ is the skew-symmetric matrix associated with the triple $\varDelta$ according to the rule (24).

It can now be seen that all previous results concerning steady states, stability and sedimentation speed carry over to the general case of a non-uniform body whose centers of mass and volume are distinct. In particular, results previously stated in terms of M_1 and M_2 now hold with D_1 in place of M_1 and D_2 in place of M_2. This conclusion follows from the fact that the leading-order solution for general bodies outlined in (79) and (80) has the same structural form as the leading-order solution for uniform bodies outlined in (15) and (16). The special case of uniform bodies is recovered when the components $\varDelta$ of the (scaled) mass eccentricity vector are zero.

Weinberger [18] proved that the leading-order dynamics of a body whose centers of mass and volume are sufficiently separated possess a steady state that is globally asymptotically stable. This result can now be seen to follow from case (1) of Theorem 4.1. In particular, by continuity of eigenvalues, and due to the fact that the skew-symmetric matrix $[\varDelta\times]$ has one real and two imaginary eigenvalues of the form $\{0, \pm i|\varDelta|\}$, we note that D_2 must have one real and a genuinely complex conjugate pair of eigenvalues whenever the norm of $\varDelta$ is sufficiently large compared to the norm of M_2 in an appropriate sense. Thus, when the center of mass and center of volume of a body are sufficiently separated, Theorem 4.1 guarantees that the leading-order body dynamics possess a unique, globally asymptotically stable, steady state.

Acknowledgments. It is a pleasure to thank Professor Hans Weinberger for his helpful comments. The following generous support is gratefully acknowledged: OG the US National Science Foundation, ABAG and JHM the Swiss National Science Foundation.

References

[1] G.K. Batchelor, Slender-body theory for particles of arbitrary cross-section in Stokes flow, *Journal of Fluid Mechanics* **44** (1970) 419–440.

[2] G. Galdi, On the motion of a rigid body in a viscous liquid: a mathematical analysis with applications, in Handbook of mathematical fluid dynamics, Volume 1, Chapter 7, Edited by S.J. Friedlander and D. Serre, Elsevier Science (2002).

[3] J. Garcia de la Torre and V.A. Bloomfield, Hydrodynamic properties of complex, rigid, biological macromolecules: theory and applications, *Quarterly Reviews of Biophysics* **14** (1981) 81–139.

[4] J. Happel and H. Brenner, *Low Reynolds Number Hydrodynamics*, Martinus Nijhoff (1983).

[5] H.J. Hinch, *Perturbation methods*, Cambridge University Press (1991).

[6] M.W. Hirsch and S. Smale, *Differential Equations, Dynamical Systems, and Linear Algebra*, Academic Press, Pure and Applied Mathematics **60** (1974).

[7] V. Katritch, J. Bednar, D. Michoud, R.G. Scharein, J. Dubochet and A. Stasiak, Geometry and physics of knots, *Nature* **384** (1996) 142–145.

[8] V. Katritch, W.K. Olson, P. Pieranski, J. Dubochet and A. Stasiak, Properties of ideal composite knots, *Nature* **388** (1997) 148–151.

[9] J.B. Keller and S.I. Rubinow, Slender-body theory for slow viscous flow, *Journal of Fluid Mechanics* **75** (1976) 705–714.

[10] S. Kim and S.J. Karrila, *Microhydrodynamics*, Butterworth-Heinemann (1991).

[11] J.E. Marsden and T.S. Ratiu, *Introduction to Mechanics and Symmetry*, Springer-Verlag, Texts in Applied Mathematics **17** (1994).

[12] P. Pieranski, In search of ideal knots, in Ideal Knots, Chapter 2, Edited by A. Stasiak, V. Katritch and L.H. Kauffman, World Scientific Publishing (1998).

[13] J. Rotne and S. Prager, Variational treatment of hydrodynamic interaction in polymers, *Journal of Chemical Physics* **50** (1969) 4831–4837.

[14] Y.G. Sinai, *Topics in Ergodic Theory*, Princeton University Press (1994).

[15] A. Stasiak, J. Dubochet, V. Katritch and P. Pieranski, Ideal knots and their relation to the physics of real knots, in Ideal Knots, Chapter 1, Edited by A. Stasiak, V. Katritch and L.H. Kauffman, World Scientific Publishing (1998).

[16] A. Stasiak, V. Katritch, J. Bednar, D. Michoud and J. Dubochet, Electrophoretic mobility of DNA knots, *Nature* **384** (1996) 122.

[17] A.V. Vologodskii, N.J. Crisona, B. Laurie, P. Pieranski, V. Katritch, J. Dubochet and A. Stasiak, Sedimentation and electrophoretic migration of DNA knots and catenanes, *Journal of Molecular Biology* **278** (1998) 1–3.

[18] H.F. Weinberger, Variational properties of steady fall in a Stokes flow, *Journal of Fluid Mechanics* **52** (1972) 321–344.

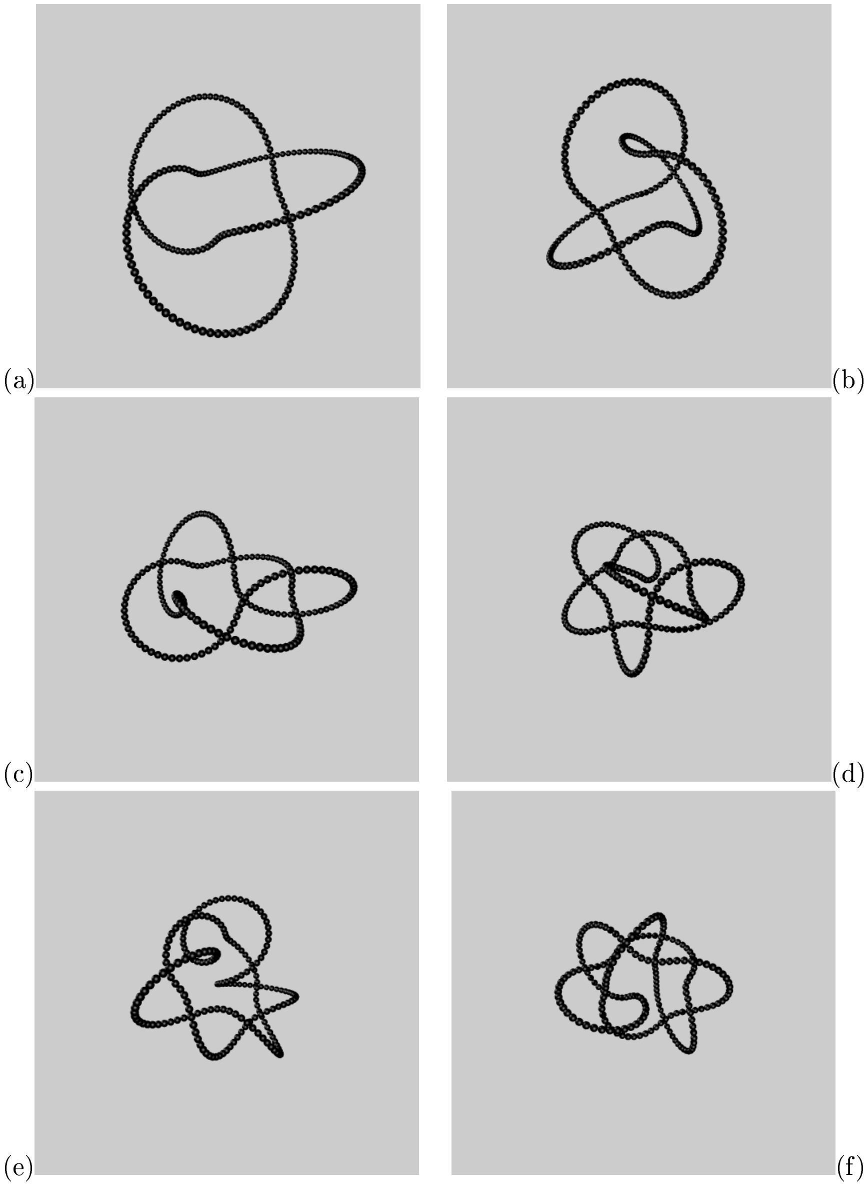

Figure 1: Models of various different knotted filaments. Each filament has unit length and is modeled by $n = 200$ identical beads of radius $\gamma = 1/400$ uniformly spaced along the filament axis. (a) - (f): approximations to ideal configurations of 3_1, 4_1, 5_1, 6_1, 7_1 and 7_7 knots based on original data of [7, 12].

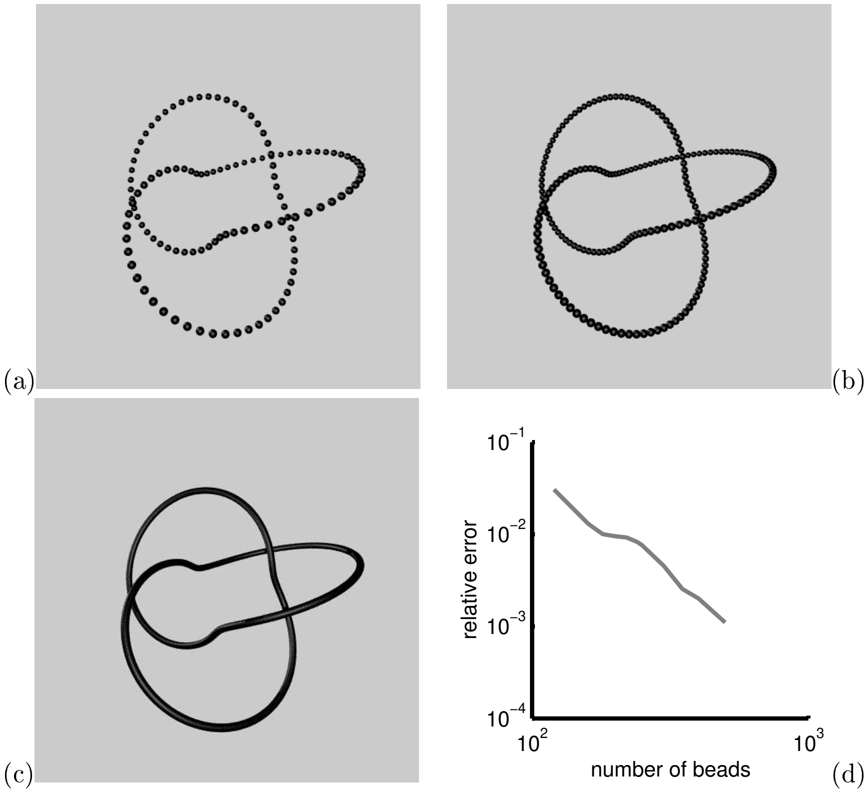

Figure 2: A continuous filament may be modeled by different numbers of identical beads of given radius, that are uniformly spaced along the filament axis. For any given number of beads the hydrodynamic resistance matrix may be computed using the Rotne-Prager approximation. (a), (b), (c): a filament of unit length modeled by $n = 120$, 200 and 750 beads of radius $\gamma = 1/400$. (d): relative error in the resistance matrix L as a function of the number n of beads.

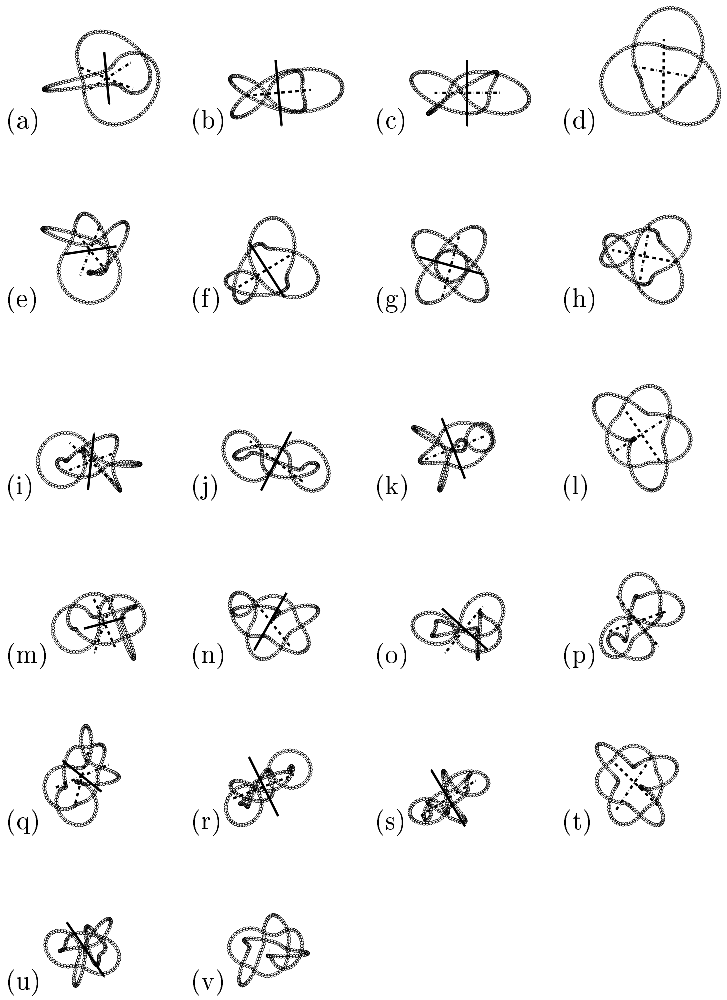

Figure 3: Hydrodynamic axes for filaments in the shapes of ideal 3_1 (a-d), 4_1 (e-h), 5_1 (i-l), 6_1 (m-p), 7_1 (q-t) and 7_7 (u,v) knots. (a),(e),(i),(m),(q): the three hydrodynamic axes defined by $\pm\eta_{\rm min}$ (dot-dashed), $\pm\eta_{\rm mid}$ (dashed) and $\pm\eta_{\rm max}$ (solid) for the 3_1, 4_1, 5_1, 6_1 and 7_1 knots. The two steady state motions associated with each axis occur when that axis is parallel to the gravitational field. (b),(f),(j),(n),(r): views parallel to the axis associated with $\pm\eta_{\rm min}$. (c),(g),(k),(o),(s): views parallel to the axis associated with $\pm\eta_{\rm mid}$. (d),(h),(l),(p),(t): views parallel to the axis associated with $\pm\eta_{\rm max}$. (u): the single hydrodynamic axis defined by $\pm\eta_{\rm real}$ for the 7_7 knot. (v): view parallel to the hydrodynamic axis for the 7_7 knot.

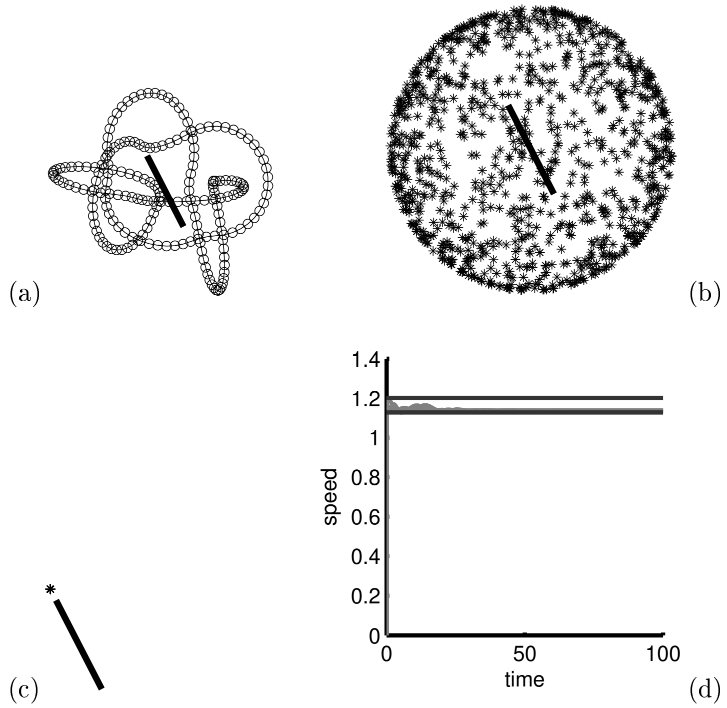

Figure 4: Sedimentation simulation for a filament in the shape of an ideal 7_7 knot. (a): the hydrodynamic axis defined by the single real eigenvector $\pm\eta_{\rm real}$ of M_2. (b): distribution of gravity directions in the body frame at $t = 0$. (c): distribution of gravity directions in the body frame at $t = 200$. The simulation was performed with the exact equations of motion (14) with $\varepsilon = 0.01$. (d): time histories of sedimentation speed ϑ for various members from the sample. The two horizontal lines in the plot correspond to the eigenvalues $\theta_{\min}$ and $\theta_{\max}$ of M_1.

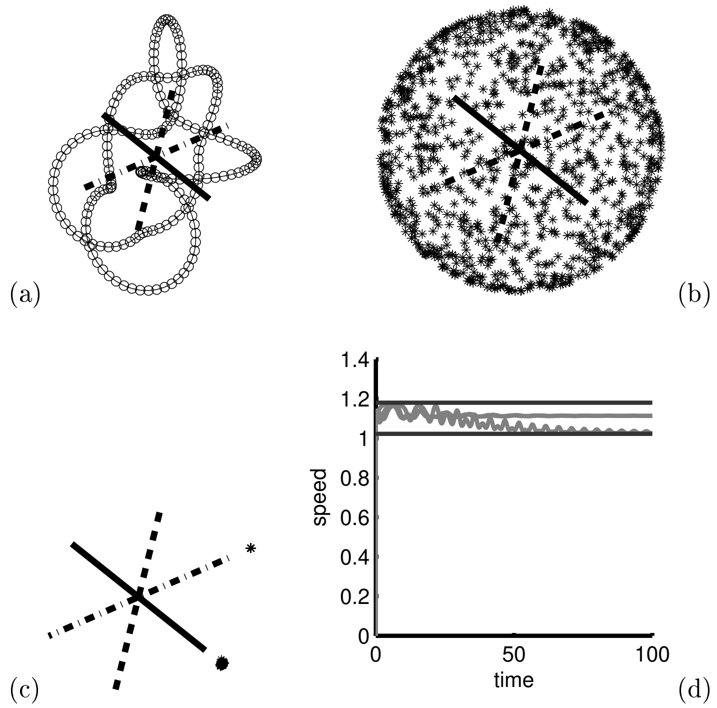

Figure 5: Sedimentation simulation for a filament in the shape of an ideal 7_1 knot. (a): the three hydrodynamic axes defined by the eigenvectors $\pm\eta_{\min}$ (dot-dashed), $\pm\eta_{\mathrm{mid}}$ (dashed) and $\pm\eta_{\max}$ (solid) of M_2. (b): distribution of gravity directions in the body frame at $t = 0$. (c): distribution of gravity directions in the body frame at $t = 200$. The simulation was performed with the exact equations of motion (14) with $\varepsilon = 0.01$. (d): time histories of sedimentation speed ϑ for various members from the sample. The two horizontal lines in the plot correspond to the eigenvalues $\theta_{\min}$ and $\theta_{\max}$ of M_1.

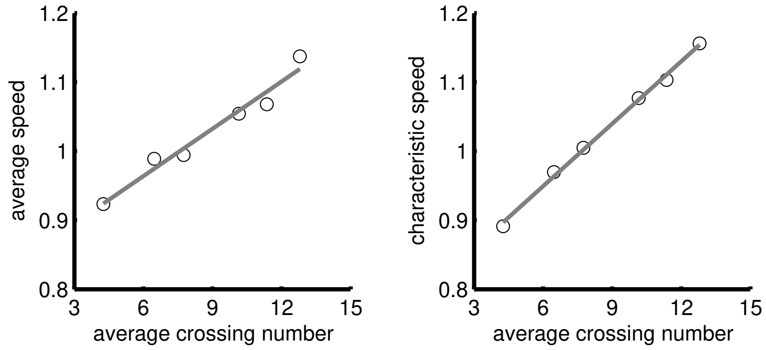

(a) (b)

Figure 6: Plots of sedimentation speed versus average crossing number for the ideal 3_1, 4_1, 5_1, 6_1, 7_1 and 7_7 knots. The data on average crossing number is taken from [15]. (a): average sedimentation speed computed from numerical simulations of each different ideal shape. In the simulations a sample of randomly oriented knots of a given shape is started from rest and their time evolution is computed using the exact equations of motion (14) with $\varepsilon = 0.01$ until the time $t = 800$. The average of the sedimentation speed ϑ over the sample is then computed and plotted against the average crossing number for that shape. (b): characteristic sedimentation speed ϑ_* for each ideal shape computed from the definition in (62). The straight lines in each plot represent best linear fits to the data points.